

Bulk Ionic Dissociation is Crucial for Understanding Chemically-Propelled Swimmers

Aidan T. Brown,^{1,*} Wilson C. K. Poon,¹ Christian Holm,² and Joost de Graaf²

¹*SUPA, School of Physics and Astronomy, The University of Edinburgh, King's Buildings, Peter Guthrie Tait Road, Edinburgh, EH9 3FD, United Kingdom*

²*Institute for Computational Physics (ICP), University of Stuttgart, Allmandring 3, 70569 Stuttgart, Germany*

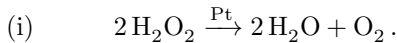
(Dated: May 29, 2022)

The effect of bulk ionic association-dissociation reactions (e.g., $\text{H}_2\text{O}_2 \rightleftharpoons \text{H}^+ + \text{HO}_2^-$) on chemical-reaction-driven colloids (swimmers) is determined using a continuum theory. We find that these bulk reactions should have a strong influence on the propulsive behavior of chemical swimmers in aqueous solution. In particular, these reactions permit charged swimmers to propel electrophoretically even if all species involved in the surface reactions are neutral. Including bulk reactions also significantly modifies the predicted speed of standard electrophoretic swimmers, by up to an order of magnitude. For swimmers whose surface reactions produce both anions and cations (ionic self-diffusiophoresis), the bulk reactions lead to an additional reactive screening length, analogous to the Debye length in electrostatics. This in turn leads to an inverse relationship between swimmer radius and swimming speed, which could explain experimental observations on Pt-polystyrene Janus swimmers.

Recent years have witnessed a boom in research on active matter [1, 2]. Of particular interest is the out-of-equilibrium physics of self-propelled particles (swimmers [3]), which exhibits a multitude of collective dynamics and phase separation behavior [4–6]. While much of this physics is generic, quantitative interpretation of experiments requires knowledge of swimmer propulsion mechanisms [7–9], which are highly system-specific. In other words, understanding how single swimmers swim is crucial for understanding their collective behavior.

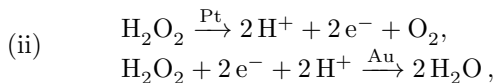
We focus here on a broad class of synthetic swimmers (and possibly biological enzymes [10, 11]) which propel via chemical gradients generated by spatially heterogeneous reactions on the swimmer surface [12–15]. Even within this class, there are (theoretically) at least three distinct propulsion mechanisms:

I: Neutral self-diffusiophoresis [15]. Neutral reactants and products are consumed and generated by a surface reaction, such as hydrogen peroxide decomposition on platinum [14]



Short-ranged interactions, such as dispersion forces [16, 17], between the molecules and the swimmer surface generate pressure gradients, and therefore fluid flow and propulsion.

II: Self-electrophoresis. Partially electrochemical surface reactions produce an ion gradient. For example, on Au-Pt bimetallic swimmers [13], reaction (i) becomes



where electrons flowing inside the conductive swimmer balance the ionic current outside. The ionic gradient

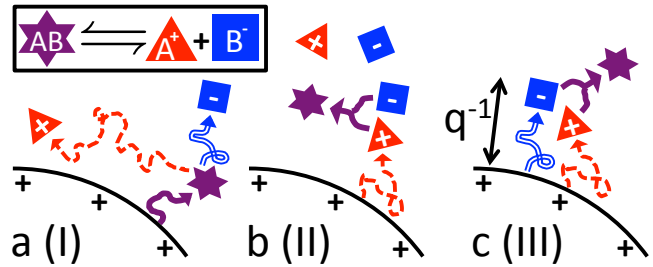
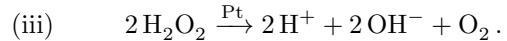


FIG. 1. Schematic illustrating the effect of a general bulk ionic association-dissociation reaction, $AB \rightleftharpoons A^+ + B^-$ (inset), on swimmers employing propulsion mechanisms I-III, producing at the surface: a) Neutral molecules (I): the difference in diffusivity between the two dissociation products produces a diffusion potential. b) Cations (II). c) Both cations and anions (III). Here, the electric fields are screened over distances greater than the mean free reactive path of the ions, q^{-1} .

(here H^+) then produces an electric field, propelling the charged swimmer.

III: Ionic self-diffusiophoresis [18]. The reaction releases both cations and anions, e.g., (hypothetically)



Here, there is no net electrical current, because the ionic production is balanced. Nevertheless, these ions can still generate electric fields; in particular, ions diffusing away at different speeds will establish a so-called ‘diffusion potential’ [19].

In practice, the situation is more complicated. Most experimental systems use aqueous solutions, and water permits ionic association-dissociation reactions of itself and its solutes, e.g., $\text{H}_2\text{O} \rightleftharpoons \text{H}^+ + \text{OH}^-$ or $\text{H}_2\text{O}_2 \rightleftharpoons \text{H}^+ + \text{HO}_2^-$. These reactions modify the bulk ionic concentration fields, Fig. 1. This in turn generates electric fields, and introduces additional electrophoretic components to each of cases I-III. However, theoretical studies typically neglect these bulk effects, treating water as a nonreactive electrolyte [20–24].

* abrown20@staffmail.ed.ac.uk

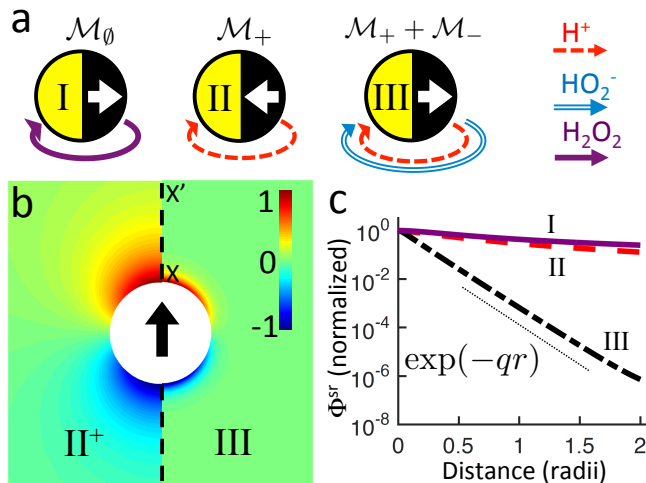


FIG. 2. (a) Schematic of the three model swimmers, corresponding to the propulsion mechanisms I-III. The white arrows indicate the direction of motion of positively charged swimmers, and colored arrows indicate solute fluxes. (b) Normalized surface-reaction-generated potential ϕ^{sr} for type II and type III propulsion. (c) Normalized radial decay of ϕ^{sr} for type I (-), II (--), and III (-.-), along $X-X'$ in b.

In this Letter, we theoretically investigate the effect of bulk ionic reactions on the speed of chemical swimmers. Speed is the most experimentally accessible parameter for a swimmer, but its prediction is challenging as it depends not just on the overall reaction rate, but also on the rate of intermediate reactions, e.g., reaction (ii). These intermediate rates are very difficult to measure for microscopic objects, and, to our knowledge, the only estimates have come by inference from the speed itself [16, 25]. As a result, these reaction rates are typically assumed to be constant, or to depend on other relevant parameters via some particular reaction mechanism [21, 24]. Similar considerations apply to the particle surface charge density σ or potential ζ . Given the notorious complexity of heterogeneous electrochemistry [26], such assumptions are unlikely to be universally valid.

Therefore, our approach here is to decouple these problematic surface properties from the effects of the bulk solvent, which we focus on. We will write the speed U of a swimmer producing and consuming one chemical species at typical surface reaction rate j^s in the form

$$U \propto \sigma j^s \mathcal{M}, \quad (1)$$

where \mathcal{M} is a dimensionless mobility parameter, which include the effects of the bulk ionic reactions. We will calculate \mathcal{M} for a basis set of model swimmers, see Fig. 2a, fuelled by H_2O_2 decomposition, and powered by the surface reaction mechanisms I-III. Though our calculations are for this specific chemical system, the model is general, and the physical principles that we highlight will also apply to different, and more complex chemical systems.

The most immediately experimentally relevant model swimmer is II, Fig. 2a, which corresponds to self-

electrophoretic bimetallic swimmers powered by H^+ currents [13]. We predict that including the bulk ionic reaction $H^+ + HO_2^- \rightleftharpoons H_2O_2$ increases the mobility parameter \mathcal{M}_{II} , and thus this swimmer's speed, up to approximately 10 times at low H^+ concentration, Fig. 3a.

In ionic diffusiophoresis (III), this same bulk reaction produces exponential screening of the potential, with a reactive screening length q^{-1} , analogous to the Debye screening length κ^{-1} in electrostatics, Fig. 2b-c. This screening induces an inverse scaling between the mobility parameter \mathcal{M}_{III} and particle radius, Fig. 3, which may underlie the hitherto unexplained [27] inverse relationship between radius and speed observed in experiments on single-catalyst Janus particles [28]. Meanwhile, bulk ionic decomposition of the neutral fuel H_2O_2 (model I) should give a small additional electrophoretic contribution for any H_2O_2 -powered swimmer, and may dominate the propulsion of swimmers with more dissociative fuels.

Finally, independent of the bulk reactions, our calculations – going beyond the usual limiting case $\kappa a \gg 1$, with a the swimmer radius – predict a universal scaling of the mobility $\mathcal{M} \propto a^3$ for small a . Experiments [29, 30], have not observed a similar scaling of the speed: this may indicate that the (as yet unmeasured) surface reaction rates are much larger for nanoswimmers than for microswimmers.

The standard model of self-electrophoresis [21, 22] involves a system of continuum equations for N solute concentration fields, c_i , the electrostatic potential ϕ , and the fluid flow \mathbf{u} . The bulk flux of each species is $\mathbf{j}_i = c_i \mathbf{u} - D_i \nabla c_i - D_i z_i e c_i \nabla \phi / (k_B T)$, with e the fundamental charge, k_B Boltzmann's constant, T temperature, D_i the diffusivity, and z_i the valency of each species. The electric potential satisfies Poisson's equation $\epsilon \nabla^2 \phi = -\rho_e$ with charge density $\rho_e = e \sum_i z_i c_i$ and constant solution permittivity ϵ . The flow field satisfies the Stokes equations $\eta \nabla^2 \mathbf{u} = \nabla p + \mathbf{f}$ and $\nabla \cdot \mathbf{u} = 0$ for low-inertia, incompressible flow, with electrostatic force density $\mathbf{f} = \rho_e \nabla \phi$, hydrostatic pressure p , and viscosity η . Without bulk reactions, conservation of chemical species requires $\nabla \cdot \mathbf{j}_i = 0$. With bulk reactions, $\nabla \cdot \mathbf{j}_i = R_i(c_1, \dots, c_N)$, where R_i specifies each species' local (bulk) formation rate.

Meanwhile, the surface reactions are specified through the surface production rates j_i^s , i.e., $\hat{\mathbf{n}} \cdot \mathbf{j}_i(\mathbf{s}) = j_i^s(\mathbf{s})$. Here, (\mathbf{s}) and $\hat{\mathbf{n}}$ indicate evaluation at, and the normal out of, the particle surface. The particle is spherical, with fluxes distributed axisymmetrically around some axis, which we label z . We model a dielectric particle with a uniform surface charge density σ and a vanishingly small internal dielectric constant, so that $\hat{\mathbf{n}} \cdot \nabla \phi(\mathbf{s}) = -\sigma/\epsilon$. Our results apply equally to a (bi)metallic particle with constant ζ , provided $\zeta = (\sigma a)/(\epsilon(1 + \kappa a))$ [31]. The particle surface is a no-slip boundary: $\mathbf{u}(\mathbf{s}) = \mathbf{0}$ in the co-moving frame. At infinity: $\mathbf{u} \rightarrow -\mathbf{U}$, with \mathbf{U} the swimmer velocity; $c_i \rightarrow c_i^\infty$, which are uniform, bulk concentrations; and $\{\phi, \rho_e, p\} \rightarrow 0$.

We linearize the continuum equations by assuming

the Debye-Hückel approximation, $\phi \ll k_B T/e$. We can then split $\phi = \phi^{\text{eq}} + \phi^{\text{sr}}$ with $\phi^{\text{eq}} = \sigma a^2 \exp[-\kappa(r-a)]/(r\epsilon(1+\kappa a))$ being the equilibrium potential due to surface charge, and ϕ^{sr} the additional non-equilibrium potential due to surface reactions. We assume $\phi^{\text{sr}} \ll \phi^{\text{eq}}$. Solving the linearized equations gives the general solution [31, 32]

$$\phi^{\text{sr}} = \sum_{j,n} \phi_{j,n}^{\text{sr}} P_n(\cos\theta) \left(\frac{a}{r}\right)^{n+1} \frac{T_n(g_j r)}{T_n(g_j a)} e^{-g_j(r-a)}, \quad (2)$$

$$T_n(x) \equiv \sum_{m=0}^n \frac{2^m n! (2n-m)!}{m! (2n)! (n-m)!} x^m, \quad (3)$$

with P_n the Legendre polynomials of order n , and θ the polar angle. Here, each of the inverse screening lengths g_j (like κ) corresponds to a distinct eigenvalue of the linear system of equations, while the surface coefficients $\phi_{j,n}^{\text{sr}}$ are determined by the boundary conditions [31]. Note that the index j refers to the (up to) $N+1$ eigenvalues, not to the N chemical species. Applying the Lorentz reciprocal theorem [33, 34], then gives the speed in the z -direction [31]

$$U = \frac{2\sigma k_B T}{3\eta e a} \sum_j \frac{\kappa - g_j}{(\kappa + g_j)^2} \phi_{j,1}^{\text{sr}} F(\kappa a, g_j a), \quad (4)$$

where, because the surface is uniformly charged, only the $n=1$ Legendre components, $\phi_{j,1}^{\text{sr}}$, contribute [35]. Here,

$$F(x, y) = \frac{(x+y)^3}{6(1+x)(1+y)} e^{x+y} \times \int_1^\infty \frac{(t-1)^2 (2t+1)}{t^5} (1+xt)(1+yt) e^{-t(x+y)} dt, \quad (5)$$

is the self-electrophoretic equivalent of Henry's function for electrophoresis in an external field [36]. However, in the limit $x+y \ll 1$, corresponding to a thick screening layer, $F(x, y) \rightarrow (x+y)^3/8$, whereas Henry's original function approaches a constant, finite value in this limit. For $x+y \gg 1$, $F(x, y) = 1$.

We now apply this theory to the simplest chemical system, a neutral fuel AB and its dissociation products, monovalent A^+ and B^- ions. The diffusivity, bulk concentration, etc. of each active species are specified by subscripts, \emptyset (for neutral), $+$, and $-$. The sole bulk reaction is $AB \rightleftharpoons A^+ + B^-$. This reaction is first order with respect to each species, with production rates, $R_\emptyset = k_{\text{as}} c_+ c_- - k_{\text{dis}} c_\emptyset$ and $R_+ = R_- = -R_\emptyset$. Here, k_{as} and k_{dis} are association and dissociation rate constants. There are also two nonreactive ions, which only contribute through charge balance, and their effect on κ [31].

This system yields a degenerate set of equations, giving only three (not six) independent eigenvalues, and hence three unique inverse screening lengths, g_j , which are: 0, corresponding to unscreened ionic currents [35]; κ , corre-

sponding to normal electrostatic screening; and an additional reactive screening term

$$q = k_{\text{as}}^{\frac{1}{2}} \left(\frac{c_+^\infty c_-^\infty}{D_\emptyset c_\emptyset^\infty} + \frac{c_+^\infty D_+ + c_-^\infty D_-}{D_+ D_-} \right)^{\frac{1}{2}}, \quad (6)$$

where q^{-1} can be interpreted as the mean free path of the reactive species before reaction in the bulk, see Fig. 1c. The speed is a sum over terms like Eq. (1),

$$U = \frac{e}{3\eta\epsilon\kappa^3 D_\emptyset} \sigma \left[j_{+,1}^s \mathcal{M}_+ + j_{-,1}^s \mathcal{M}_- + j_{\emptyset,1}^s \mathcal{M}_\emptyset \right]. \quad (7)$$

Without bulk reactions we have $\mathcal{M}_\emptyset = 0$ (no electrophoresis for purely neutral reactions) and $\mathcal{M}_\pm = \mp F(\kappa a, 0) D_\emptyset / D_\pm$. With bulk reactions, for weak dissociation $c_\emptyset^\infty \gg \{c_+^\infty, c_-^\infty\}$,

$$\mathcal{M}_\emptyset = -\frac{\beta c_+^\infty c_-^\infty \tilde{D}}{c_\emptyset^\infty \tilde{c}^\infty D^*} [\Theta F(\kappa a, qa) - F(\kappa a, 0)], \quad (8)$$

$$\mathcal{M}_\pm = \frac{D_\emptyset}{D^*} \left[\beta \Theta \frac{c_\mp^\infty \tilde{D}}{D_\pm \tilde{c}^\infty} F(\kappa a, qa) \mp F(\kappa a, 0) \right], \quad (9)$$

where $\tilde{D} = (D_+ + D_-)/2$ and $\tilde{c}^\infty = (c_+^\infty + c_-^\infty)/2$; $D^* = (D_+ c_+^\infty + D_- c_-^\infty)/(c_+^\infty + c_-^\infty)$ is the concentration-averaged diffusivity; $\beta = (D_+ - D_-)/(D_+ + D_-)$ is the prefactor for the diffusion potential [19]; and we absorb the screening factors in

$$\Theta = \left(\frac{\kappa}{\kappa + q} \right)^3 \frac{2(aq + 1)}{(aq)^2 + 2aq + 2}. \quad (10)$$

We now insert experimentally realistic parameters for H_2O_2 powered swimmers. H_2O_2 (AB) dissociates into H^+ (A^+) and HO_2^- (B^-) ions, with $D_{\text{H}^+} = 9.3 \times 10^{-9} \text{ m}^2\text{s}^{-1}$ [37], $D_{\text{HO}_2^-} = 0.9 \times 10^{-9} \text{ m}^2\text{s}^{-1}$ [38], and $D_{\text{H}_2\text{O}_2} = 1.7 \times 10^{-9} \text{ m}^2\text{s}^{-1}$ [39]. The unreactive ions, Na^+ and Cl^- , have bulk concentrations $c_{\text{Na}^+}^\infty$ and $c_{\text{Cl}^-}^\infty$, and the remaining concentrations are determined by charge balance, $c_{\text{H}^+}^\infty + c_{\text{Na}^+}^\infty = c_{\text{HO}_2^-}^\infty + c_{\text{Cl}^-}^\infty$, and the equilibrium $c_{\text{H}^+}^\infty c_{\text{HO}_2^-}^\infty = K_{\text{eq}} c_{\text{H}_2\text{O}_2}^\infty$. Here, $K_{\text{eq}} = k_{\text{dis}}/k_{\text{as}} = 2.5 \times 10^{-12} \text{ M}$ [31, 40]. We estimate $k_{\text{as}} = 4.9 \times 10^{10} \text{ M}^{-1}\text{s}^{-1}$ using the Smoluchowski-Debye theory for diffusion limited reactions [31, 41]. Our base parameters, used unless specified otherwise, are $c_{\text{Na}^+}^\infty = c_{\text{Cl}^-}^\infty = 1 \text{ mM}$, $a = 500 \text{ nm}$, and $c_{\text{H}_2\text{O}_2}^\infty = 3 \text{ M}$. For these parameters, $\beta = 0.8$, $q^{-1} = 70 \text{ nm}$, $\kappa^{-1} = 10 \text{ nm}$, and $c_{\text{H}^+}^\infty = c_{\text{HO}_2^-}^\infty = (K_{\text{eq}} c_{\text{H}_2\text{O}_2}^\infty)^{1/2} = 3 \times 10^{-6} \text{ M}$.

Since the various fluxes are linearly independent, we consider here only three basic model swimmers, Fig. 2a. I and II have fluxes of single species, AB and A^+ respectively, and mobilities $\mathcal{M}_I = \mathcal{M}_\emptyset$ and $\mathcal{M}_{II} = \mathcal{M}_+$. III has equal fluxes of A^+ and B^- ions, and mobility $\mathcal{M}_{III} = \mathcal{M}_+ + \mathcal{M}_-$. For these model swimmers, only the $n=1$ mode of each flux is present, i.e., $j_i^s \propto \cos\theta$. Type

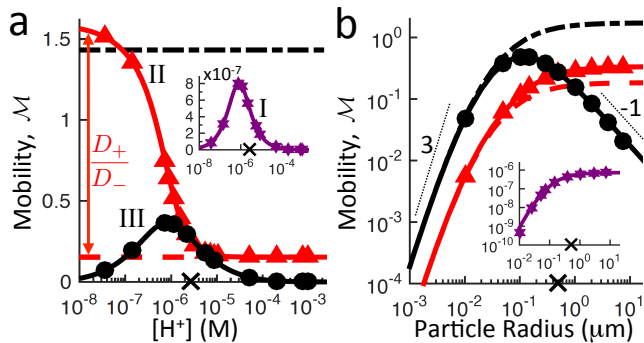


FIG. 3. Dimensionless mobilities for type I (\star , insets), II (\blacktriangle), and III (\bullet) propulsion, from analytical theory with (solid curves) and without (broken curves) bulk reactions; and FEM simulations (symbols). \times indicates the base parameter set defined in text. For a) $[H^+]$, at fixed κ , b) particle radius.

II propulsion corresponds closely to the standard model of proton-powered, bimetallic swimmers [42]. Since H_2O_2 is much more acidic than H_2O , the dissociation of water, which we neglect here, should contribute little to the ionic gradients for this swimmer.

Figure 2b-c plots the reaction-generated potential ϕ^{sr} for these model swimmers (I, not shown, is similar to II). For type III propulsion, $\phi \propto \exp[-q(r-a)]$, Fig. 2c: because there is no net electric current, the electric field does not extend beyond the mean-free path of the released ions. The other swimmers have $\phi \propto r^{-2}$. We expect this difference in the range of the electrostatic potential to lead to different swimmer-swimmer and swimmer-surface interactions [7, 8, 43], which future work will study.

Here, we focus on how the dimensionless mobilities depend on the proton concentration $[H^+]$ and swimmer radius a , Fig. 3. Other relevant variables, like H_2O_2 and salt concentration, are not studied here, because including bulk reactions does not significantly modify their effect. To verify our analytical theory, we performed finite-element method (FEM) calculations, without linearization, but with sufficiently low fluxes and charge density to remain in the linear regime. We also checked that the analytical calculations continue to apply semi-quantitatively even for non-linear, experimentally realistic surface parameters. For further details and parameter values, see [31].

The effect of the bulk reactions is highlighted most clearly by varying $[H^+]$, Fig. 3a. Without bulk reactions, the type II mobility is independent of $[H^+]$ (red broken line), and is just inversely proportional to the mobility of the current-carrying ion, here D_{H^+} . Including bulk reactions (solid curve) increases the mobility at low $[H^+]$ by changing the identity of this current-carrying ion. The large excess of HO_2^- ions at low H^+ react immediately with any protons released. The protons are thus replaced by HO_2^- ions flowing in the opposite direction. Hence, $\mathcal{M}_{\text{II}} \propto 1/D_{\text{HO}_2^-}$, not $1/D_{H^+}$, increasing the swimmer

mobility $D_{H^+}/D_{\text{HO}_2^-} \sim 10$ times (red arrow). At high $[H^+]$, the current remains entirely H^+ dominated, so the mobility decreases towards the no-bulk-reactions value.

Meanwhile, the bulk reactions enable type I propulsion, through dissociation of the neutral fuel ($\mathcal{M}_0 = 0$ without bulk reactions), but suppress type III propulsion through ionic recombination. At either end of the $[H^+]$ range, there are so many H^+ or HO_2^- ions in the bulk that the ions produced by these swimmers react immediately, and therefore cannot set up a diffusion potential. This explains the peaks in \mathcal{M}_0 and \mathcal{M}_{III} at intermediate $[H^+]$. The peaks correspond to the maximum reactive mean-free path q^{-1} , at $c_+^\infty = (c_\theta^\infty K_{\text{eq}} D_- / D_+)^{1/2}$. Provided swimmer surface properties remain approximately constant, we expect all these trends to be reflected in the speed of real swimmers. In particular, we predict a large speed increase for bimetallic (type II) swimmers at low $[H^+]$ (high pH).

The radius a has two distinct effects on the mobilities, Fig. 3b. First, even without bulk reactions, the function F , Eq. (5) causes all mobilities to scale as a^3 for small radius, $\{\kappa a, qa\} \ll 1$. Experimentally, however, nanoswimmers appear to be as fast or faster than microswimmers [29, 30], e.g., $600 \mu\text{ms}^{-1}$ for $a = 15 \text{ nm}$ Au-Pt swimmers [30] compared to $1 - 10 \mu\text{ms}^{-1}$ for similar microswimmers [9, 44]. These experiments are not directly comparable, but there is a striking discrepancy between the trend of these results and our predictions for the relevant mobility \mathcal{M}_{II} . A possible resolution is that the (as yet unmeasured) ionic surface reaction rates may be much higher for the nanoswimmers than for the microswimmers: measurement of these reaction rates is therefore essential for further progress. Alternatively, other mechanisms [45], or non-continuum effects [46] may come into play for nanoswimmers.

Second, for large ($qa \gg 1$) type III swimmers, $\mathcal{M}_{\text{III}} \propto 1/a$, due to the reactive e^{-qr} screening of the potential. A scaling of $U \propto a^{-1}$ has been observed for some bimetallic [44], and single catalyst microswimmers [28]. Type II is currently the preferred mechanism for these swimmers [16, 21, 24], but this $1/a$ scaling suggests an alternative type III mechanism, corresponding to reaction (iii). This is plausible, since even non-electrochemical H_2O_2 decomposition on Pt can release ions [47]. This mechanism would also avoid the conceptual difficulty of producing a net ionic current in single-catalyst systems [16, 24]. Full evaluation of this possibility mechanism requires solution of the complete H_2O_2 - H_2O reaction system, which goes beyond the scope of this work.

Finally, type I electrophoresis relies on the (low) dissociation rate of the neutral fuel to generate an ionic gradient. Hence, it is always less efficient than the other mechanisms, by a factor $\sim (K_{\text{eq}}/c_\theta^\infty)^{1/2}$, which is $\sim 10^{-6}$ here. However, since the overall, neutral flux may be much larger than the intermediate, ionic fluxes, type I propulsion could still be significant. We calculate [31] that it could account for $\sim 5\%$ of the observed speed of the Pt-polystyrene swimmers studied in Ref. [16]. Hence, this

model cannot explain the propulsion of H_2O_2 -powered swimmers, and focussing just on the type II and III mechanisms for these swimmers is justified. However, for fuels with higher dissociation constants, e.g., hydrazine [48], electrophoresis generated by neutral type I could become the dominant mechanism.

In conclusion, we have shown that bulk ionic dissociation should have a strong effect on all chemically-propelled swimmers in aqueous solutions. In particular, we predict: an order of magnitude speed increase for some proton-powered bimetallic swimmers; an additional reactive screening length, analogous to the Debye length in electrostatics; and electrophoretic contributions to the propulsion of swimmers with purely neutral surface reactions. Our results should encourage future experimental work on chemical swimmers, and in particular, on the difficult but necessary task of measuring ionic surface reaction rates *in situ*. Further theoretical work will focus on applying our calculations to fully realized experimen-

tal systems, e.g., mixed metal-dielectric swimmers, and investigating the effect of bulk reactions on swimmer-swimmer and swimmer-surface interactions.

ACKNOWLEDGMENTS

This work was funded by UK EPSRC grant EP/J007404/1 (WP); ERC Advanced Grant ERC-2013-AdG 340877-PHYSAP (AB and WP); NWO Rubicon Grant #680501210 (JdG); and DFG SPP 1726 ‘Microswimmers – from single particle motion to collective behavior’ (JdG and CH). We thank Patrick Kreissl for checking many of the calculations; and Michael Kuron, Georg Rempfer, Joakim Stenhammar, Mike Cates, Alexander Morozov, and Teun Visser for useful comments on the manuscript.

-
- [1] S. Ramaswamy, *Annu. Rev. Condens. Matter Phys.* **1**, 323 (2010).
- [2] M. C. Marchetti et al., *Rev. Mod. Phys.* **85**, 1143 (2014).
- [3] W. C. K. Poon, From *Clarkia* to *Escherichia* and janus: The physics of natural and synthetic active colloids, in *Physics of Complex Colloids*, edited by C. Bechinger, F. Sciortino, and P. Zihler, pages 317–386, Società Italiana di Fisica, Bologna, 2013.
- [4] J. Schwarz-Linek et al., *Proc. Natl. Acad. Sci. USA* **109**, 4052 (2012).
- [5] J. Palacci, S. Sacanna, A. P. Steinberg, D. J. Pine, and P. M. Chaikin, *Science* **339**, 936 (2013).
- [6] A. Bricard, J.-B. Caussin, N. Desreumaux, O. Dauchot, and D. Bartolo, *Nature* **503**, 95 (2013).
- [7] A. T. Brown et al., *Soft Matter Advance Article*, DOI: 10.1039/C5SM01831E (2015).
- [8] F. Ginot et al., *Phys. Rev. X* **5**, 011004 (2015).
- [9] I. Theurkauff, C. Cottin-Bizonne, J. Palacci, C. Ybert, and L. Bocquet, *Phys. Rev. Lett.* **108**, 268303 (2012).
- [10] H. S. Muddana, S. Sengupta, T. E. Mallouk, A. Sen, and P. J. Butler, *J. Am. Chem. Soc.* **132**, 2110 (2010).
- [11] S. Sengupta et al., *J. Am. Chem. Soc.* **135**, 1406 (2013).
- [12] S. J. Ebbens and J. R. Howse, *Soft Matter* **6**, 726 (2010).
- [13] W. F. Paxton et al., *J. Am. Chem. Soc.* **126**, 13424 (2004).
- [14] J. R. Howse et al., *Phys. Rev. Lett.* **99**, 048102 (2007).
- [15] R. Golestanian, T. B. Liverpool, and A. Ajdari, *Phys. Rev. Lett.* **94**, 220801 (2005).
- [16] A. T. Brown and W. C. K. Poon, *Soft Matter* **10**, 4016 (2014).
- [17] J. de Graaf, G. Rempfer, and C. Holm, *IEEE Trans. Nanobiosci.* **14**, 272 (2015).
- [18] M. Ibele, T. E. Mallouk, and A. Sen, *Angew. Chem. Int. Ed.* **48**, 3308 (2009).
- [19] J. L. Anderson, *Ann. Rev. Fluid Mech.* **21**, 61 (1989).
- [20] J. Moran, P. Wheat, and J. Posner, *Phys. Rev. E* **81**, 065302 (2010).
- [21] J. L. Moran and J. D. Posner, *J. Fluid Mech.* **680**, 31 (2011).
- [22] B. Sabass and U. Seifert, *J. Chem. Phys.* **136**, 214507 (2012).
- [23] J. L. Moran and J. D. Posner, *Phys. Fluids* **26**, 042001 (2014).
- [24] S. Ebbens et al., *Euro. Phys. Lett.* **106**, 58003 (2014).
- [25] W. F. Paxton et al., *J. Am. Chem. Soc.* **128**, 14881 (2006).
- [26] E. Gileadi, *Physical Electrochemistry: Fundamentals, Techniques and Applications*, Wiley-VCH Weinheim, Germany, 2011.
- [27] This scaling was originally explained by postulating a diffusion limited reaction [28], which does not apply in practice [16].
- [28] S. Ebbens, M.-H. Tu, J. R. Howse, and R. Golestanian, *Phys. Rev. E* **85**, 020401 (2012).
- [29] M. Xuan, J. Shao, X. Lin, L. Dai, and Q. He, *ChemPhysChem* **15**, 2255 (2014).
- [30] T.-C. Lee et al., *Nano Lett.* **14**, 2407 (2014).
- [31] A. T. Brown, W. C. K. Poon, C. Holm, and J. de Graaf, *Supplementary Material*, <http://prl.aps.org/>, 2015.
- [32] J. Y. Kim and B. J. Yoon, *J. Colloid Interf. Sci.* **262**, 101 (2003).
- [33] B. Sabass and U. Seifert, *J. Chem. Phys.* **136**, 064508 (2012).
- [34] M. Teubner, *J. Chem. Phys.* **76**, 5564 (1982).
- [35] R. Golestanian, T. B. Liverpool, and A. Ajdari, *New J. Phys.* **9**, 126 (2007).
- [36] D. Henry, *Proc. Roy. Soc. Lond. A Mat.* **133**, 106 (1931).
- [37] W. M. Haynes, editor, *CRC handbook of chemistry and physics, 93rd ed.*, CRC press, Boca Raton, U.S.A., 2013.
- [38] F. van den Brink, W. Visscher, and E. Barendrecht, *J. Electroanal. Chem.* **172**, 301 (1984).
- [39] D. M. H. Kern, *J. Am. Chem. Soc.* **76**, 4208 (1954).
- [40] A. J. Everett and G. J. Minkoff, *Trans. Faraday Soc.* **49**, 410 (1953).
- [41] E. Caldin, *Fast reactions in solution*, Blackwell Scientific Publications, Oxford, 1964.
- [42] W. F. Paxton, A. Sen, and T. E. Mallouk, *Chem.-Eur. J.* **11**, 6462 (2005).

- [43] W. E. Uspal, M. N. Popescu, S. Dietrich, and M. Tasinkevych, *Soft Matter* **11**, 434 (2015).
- [44] P. M. Wheat, N. A. Marine, J. L. Moran, and J. D. Posner, *Langmuir* **26**, 13052 (2010).
- [45] R. Golestanian, *Phys. Rev. Lett.* **115**, 108102 (2015).
- [46] J. F. Brady, *J. Fluid. Mech.* **667**, 216 (2011).
- [47] Y. Ono, T. Matsumura, N. Kitajima, and S. Fukuzumi, *J. Phys. Chem.* **81**, 1307 (1977).
- [48] W. Gao, A. Pei, R. Dong, and J. Wang, *J. Am. Chem. Soc.* **136**, 2276 (2014).

Bulk Ionic Dissociation is Crucial for Understanding Chemically-Propelled Swimmers Supplementary Material

Aidan T. Brown,^{1,*} Wilson C. K. Poon,¹ Christian Holm,² and Joost de Graaf²

¹*SUPA, School of Physics and Astronomy, The University of Edinburgh,
King's Buildings, Peter Guthrie Tait Road, Edinburgh, EH9 3FD, United Kingdom*

²*Institute for Computational Physics (ICP), University of Stuttgart, Allmandring 3, 70569 Stuttgart, Germany
(Dated: May 29, 2022)*

I. THE MODEL

For convenience, we repeat here the governing equations of the electrophoretic model from the main text. Note that the Einstein summation convention is not used in this document. Given the concentration field of each chemical, c_i , the electrostatic potential ϕ , and fluid flow field \mathbf{u} , the flux \mathbf{j}_i of each species is

$$\mathbf{j}_i = \mathbf{u}c_i - D_i \nabla c_i - \frac{D_i z_i e c_i}{k_B T} \nabla \phi, \quad (\text{S1})$$

with e the fundamental charge, k_B Boltzmann's constant, T temperature, D_i the diffusivity, and z_i the valency of each species. Chemical reactions are specified via the local production rate $R_i(c_1, c_2, \dots, c_N)$ of each species, and chemical conservation requires

$$\nabla \cdot \mathbf{j}_i = R_i. \quad (\text{S2})$$

The electrostatic potential satisfies the Poisson equation

$$\nabla^2 \phi = -\frac{\rho_e}{\epsilon}, \quad (\text{S3})$$

with charge density, ρ_e given by

$$\rho_e = e \sum_i z_i c_i. \quad (\text{S4})$$

and solution permittivity ϵ . Finally, the fluid flow field satisfies the low inertia (low Reynolds number) Stokes equations

$$\begin{aligned} \eta \nabla^2 \mathbf{u} &= \nabla p + \mathbf{f}, \\ \nabla \cdot \mathbf{u} &= 0, \end{aligned} \quad (\text{S5})$$

with electrostatic force density $\mathbf{f} = \rho_e \nabla \phi$, hydrostatic pressure p , and viscosity η .

The surface reactions are specified by normal fluxes j_i^s of each species through the particle surface

$$\hat{\mathbf{n}} \cdot \mathbf{j}_i(\mathbf{s}) = j_i^s, \quad (\text{S6})$$

where (\mathbf{s}) and $\hat{\mathbf{n}}$ indicate evaluation at, and the normal out of, the particle surface, respectively. For the electrostatic potential, we apply a Neumann boundary condition

$$\hat{\mathbf{n}} \cdot \nabla \phi(\mathbf{s}) = -\frac{\sigma}{\epsilon}, \quad (\text{S7})$$

with surface charge density σ . We also apply a no-slip boundary condition on the particle surface

$$\mathbf{u}(\mathbf{s}) = \mathbf{0}. \quad (\text{S8})$$

Far from the swimmer, the concentrations approach uniform, bulk values c_i^∞ ; we set $\phi \rightarrow 0$, $\rho_e \rightarrow 0$, and $p \rightarrow p^\infty$, the atmospheric pressure; and, in the comoving frame, $\mathbf{u} \rightarrow -\mathbf{U}$, where \mathbf{U} is the swimmer velocity in the lab frame.

It should be remarked here that in the above theory we make the dilute-limit approximation (DLA), see Eq. (S1), which is standard in self-phoretic theories [1, 2]. The validity of this approximation has been considered for self-diffusiophoresis in Ref. [3]. The authors of Ref. [3] show that significant deviations from the DLA result can occur when (inequal) solute and solvent masses are taken into account. This necessitates the incorporation of cross-species diffusion terms in the chemical fluxes (S1). These mass terms are weighted with gradients of the concentrations. When these gradients are small, the DLA is justified. We have relatively small gradients here, as there is only a small surface production/consumption rate of the species that drive the particle out-of-equilibrium.

II. LINEARIZATION OF THE MODEL

We now linearize this model around the background situation of a quiescent fluid with homogenous potential and concentration fields: $\phi = 0$, $\mathbf{j}_i = \mathbf{0}$, $\mathbf{u} = \mathbf{0}$, $c_i = c_i^\infty$, and $p = p^\infty$. For notational convenience, we define a dimensionless parameter y_i by combining the potential and concentration fields

$$y_i = \begin{cases} \frac{e\phi}{k_B T}, & i = 0, \\ \frac{c_i - c_i^\infty}{c_i^\infty}, & i = 1, 2, \dots, N. \end{cases} \quad (\text{S9})$$

The background situation corresponds to $y_i = 0$, and to linearize, we take $y_i \ll 1$. The electrostatic component of this approximation, $y_0 = e\phi/(k_B T) \ll 1$, is just the usual Debye-Hückel approximation. Next, we perform a Taylor expansion of the reaction rates, truncating at linear order in y_i

$$R_i = \sum_{k=1}^N k_{ik} y_k, \quad i = 1, 2, \dots, N, \quad (\text{S10})$$

* abrown20@staffmail.ed.ac.uk

where the coefficients of the linear term are

$$k_{ik} = \left. \frac{\partial R_i}{\partial y_k} \right|_{\{y_l\}=0}. \quad (\text{S11})$$

Linearizing Eq. (S1)-(S3) similarly yields

$$\nabla^2 y_i = \begin{cases} -\frac{e^2}{\epsilon k_B T} \sum_{k=1}^N z_k c_k^\infty y_k, & i = 0, \\ -z_i \nabla^2 y_0 - \frac{1}{D_i c_i^\infty} \sum_{k=1}^N k_{ik} y_k, & i = 1, 2, \dots, N. \end{cases} \quad (\text{S12})$$

where the fluid velocity has been removed from the linearized equations because it scales at least quadratically with the small parameter y_i . In other words, the advection term is not relevant because we are working at low Péclet number.

Equation (S12) represents a system of $N + 1$ linear equations. However, several of the species, typically inactive ions such as Na^+ or Cl^- , may not be involved in any bulk or surface reactions, and we will now show that these inactive species can be eliminated. With N' reactive species, where $N' < N$, we specify that the first N' indices correspond to the reactive species. For the remaining, unreactive species, all the bulk reaction coefficients, k_{ik} are zero, and there is no surface flux, so Eq. (S12) can only be satisfied if

$$y_i = -z_i y_0, \quad i > N'. \quad (\text{S13})$$

This is the linear approximation to the Boltzmann distribution, which one expects, since these unreactive species should be in equilibrium. Using Eq. (S13), these ions can be eliminated from the rest of Eq. (S12) to yield

$$\kappa^{-2} \nabla^2 y_i = \begin{cases} -\sum_{k=1}^{N'} \frac{\chi_k y_k}{z_k} + \left(1 - \sum_{k=1}^{N'} \chi_k\right) y_0, & i = 0, \\ \sum_{k=1}^{N'} \left(\frac{z_i \chi_k}{z_k} - \frac{k_{ik} \kappa^{-2}}{D_i c_i^\infty} \right) y_k - z_i \left(1 - \sum_{k=1}^{N'} \chi_k\right) y_0, & i = 1, 2, \dots, N', \end{cases} \quad (\text{S14})$$

where κ is the inverse Debye screening length

$$\kappa = \left(4\pi l_B \sum_{k=1}^N z_k^2 c_k^\infty \right)^{\frac{1}{2}}. \quad (\text{S15})$$

with the Bjerrum length, $l_B = e^2/(4\pi\epsilon k_B T)$, and where χ_i is a dimensionless ionicity

$$\chi_i = 4\pi l_B \kappa^{-2} z_i^2 c_i^\infty. \quad (\text{S16})$$

Eliminating the inactive ions makes it clear that the motion of the swimmer cannot depend on the diffusivity of these ions, and is only affected by them through the value of κ and through charge balance. This is why the speed of simulated self-electrophoretic swimmers has been found to depend only on the ionicity of the supporting electrolyte, not on its conductivity [4].

Finally, linearizing the boundary conditions in Eq. (S6)-(S7) gives

$$\begin{aligned} \hat{\mathbf{n}} \cdot (\nabla y_i(\mathbf{s}) + z_i \nabla y_0(\mathbf{s})) &= -\frac{j_i^s}{D_i c_i^\infty}, \\ \hat{\mathbf{n}} \cdot \nabla y_0(\mathbf{s}) &= -\frac{\sigma e}{k_B T \epsilon}. \end{aligned} \quad (\text{S17})$$

III. LINEARIZED ELECTROSTATIC POTENTIAL

The electrostatic potential and chemical concentration fields can now be determined. The propulsion speed will be obtained in Section V.

Equation (S14) has the form of a matrix equation with components corresponding to the chemical concentrations and the electrostatic potential, so it is convenient to introduce some additional matrix notation. The bold font is reserved for real-space vectors, such as the fluid velocity \mathbf{u} , while vectors in the concentration-potential space will be underlined. A general vector \underline{t} will have $N' + 1$ components labelled t_i , while a matrix \underline{T} will have $(N' + 1) \times (N' + 1)$ components labelled \underline{T}_{ij} . A point in the concentration-potential space is specified by the vector \underline{y} , with components y_i , as defined in Eq. (S9). Using this notation, we can rewrite Eq. (S14) as

$$\nabla^2 \underline{y} = \underline{M} \underline{y}, \quad (\text{S18})$$

which can be solved by finding the $N' + 1$ eigenvectors of the matrix \underline{M} , with eigenvalues μ_j . These eigenvectors define a new basis, in which \underline{M} is diagonal. Defining \underline{w}

as the representation of \underline{y} in this basis, we have

$$\nabla^2 \underline{w} = \underline{G}^2 \underline{w}, \quad (\text{S19})$$

where the matrix \underline{G} is diagonal, with components $G_{ij} = \delta_{ij} g_j$, where δ_{ij} is the Kronecker delta and $g_j = \sqrt{\mu_j}$ are the inverse screening lengths described in the main text. For clarity, we will use the index j to refer to the screening lengths, and the indices i or k to refer to the concentrations and potentials, even where these are dummy indices.

Equation (S19) is a series of $N' + 1$ independent Helmholtz equations, and the full solution to this equation is just a vector of individual solutions to the Helmholtz equation. In spherical polar coordinates, these solutions have the form [5]

$$w_j = \sum_n w_{j,n} P_n(\cos \theta) \left(\frac{a}{r}\right)^{n+1} \frac{T_n(g_j r)}{T_n(g_j a)} e^{-g_j(r-a)}, \quad (\text{S20})$$

with $w_{j,n}$ an undetermined surface coefficient, P_n the Legendre polynomials of order n [6], θ the polar angle, and [5]

$$T_n(x) = \sum_{m=0}^n \frac{2^m n! (2n-m)!}{m! (2n)! (n-m)!} x^m. \quad (\text{S21})$$

We refer to the Legendre components by the subscript n throughout, and where we have multiple subscripts, the Legendre subscript shall be preceded by a comma. Transforming back into the original coordinate frame linearly combines the solutions in Eq. (S20), so that the final form for the electrostatic potential is

$$\phi = \sum_{j,n} \phi_{j,n} P_n(\cos \theta) \left(\frac{a}{r}\right)^{n+1} \frac{T_n(g_j r)}{T_n(g_j a)} e^{-g_j(r-a)}, \quad (\text{S22})$$

with analogous expressions for each concentration field. Here, $\phi_{j,n}$ are surface coefficients to be determined from the boundary conditions. We do this in the following section.

Finally, we write $\phi = \phi^{\text{eq}} + \phi^{\text{sr}}$, where $\phi^{\text{eq}} = \phi(\{j_i^s\} \rightarrow 0)$ is the equilibrium potential distribution without any surface chemical reactions (here, $\{j_i^s\}$ is the complete set of surface fluxes), and $\phi^{\text{sr}} = \phi(\sigma \rightarrow 0)$ is the additional potential generated by the surface reactions. Just as for the total potential ϕ , we can write

$$\phi^{\text{eq}} = \sum_{j,n} \phi_{j,n}^{\text{eq}} P_n(\cos \theta) \left(\frac{a}{r}\right)^{n+1} \frac{T_n(g_j r)}{T_n(g_j a)} e^{-g_j(r-a)}, \quad (\text{S23})$$

$$\phi^{\text{sr}} = \sum_{j,n} \phi_{j,n}^{\text{sr}} P_n(\cos \theta) \left(\frac{a}{r}\right)^{n+1} \frac{T_n(g_j r)}{T_n(g_j a)} e^{-g_j(r-a)}. \quad (\text{S24})$$

IV. SURFACE POTENTIAL COEFFICIENTS

Transformation back into the original coordinate system can be achieved using the transformation matrix \underline{K}

$$\underline{y} = \underline{K} \underline{w}, \quad (\text{S25})$$

where each element K_{ij} of \underline{K} is equal to the i^{th} component (in the original coordinate system) of the j^{th} eigenvector. Applying this transformation to Eq. (S20) gives

$$y_i = \sum_{j,n} K_{ij} w_{j,n} P_n(\cos \theta) \left(\frac{a}{r}\right)^{n+1} \frac{T_n(g_j r)}{T_n(g_j a)} e^{-g_j(r-a)}. \quad (\text{S26})$$

The boundary conditions specified in Eq. (S17) can also be rearranged into a matrix equation

$$\underline{B} \hat{\mathbf{n}} \cdot \nabla \underline{y} \Big|_{r=a} = \underline{b}, \quad (\text{S27})$$

where \underline{b} is a vector specifying each of the boundary fluxes or charge density. We define the harmonic components \underline{b}_n of \underline{b} by $\underline{b} = \sum_n P_n(\cos \theta) \underline{b}_n$, with analogous expressions defining \underline{B}_n . The solution to the boundary conditions is found by inverting Eq. (S27) to yield

$$\underline{w}_n = \underline{L}_n \underline{b}_n, \quad (\text{S28})$$

where

$$\underline{L}_n = \left[\underline{B}_n \underline{K} \underline{D}_n \right]^{-1}, \quad (\text{S29})$$

in which the diagonal matrix \underline{D}_n has elements

$$D_{ij,n} = \delta_{ij} \left[g_j \frac{\partial \log T_n(x)}{\partial x} \Big|_{x=g_j a} - \left(\frac{n+1}{a} + g_j \right) \right]. \quad (\text{S30})$$

Inserting the boundary conditions into Eq. (S26) then gives expressions of the form

$$y_i = \sum_{j,n} y_{ij,n} P_n(\cos \theta) \left(\frac{a}{r}\right)^{n+1} \frac{T_n(g_j r)}{T_n(g_j a)} e^{-g_j(r-a)}, \quad (\text{S31})$$

where the surface coefficients are

$$y_{ij,n} = K_{ij} \sum_k L_{jk,n} b_{k,n}. \quad (\text{S32})$$

In particular, this yields for the surface coefficients of the electrostatic potential (for which the index $i = 0$)

$$\phi_{j,n} = \frac{k_B T}{e} K_{0j} \sum_k L_{jk,n} b_{k,n}. \quad (\text{S33})$$

We can also determine the components ϕ^{eq} and ϕ^{sr}

$$\phi_{j,n}^{\text{eq}} = \frac{k_B T}{e} K_{0j} \sum_k L_{jk,n} b_{k,n}^{\text{eq}}. \quad (\text{S34})$$

$$\phi_{j,n}^{\text{sr}} = \frac{k_B T}{e} K_{0j} \sum_k L_{jk,n} b_{k,n}^{\text{sr}}. \quad (\text{S35})$$

where $\underline{b}^{\text{eq}} = \underline{b}(\{j_k^s\} \rightarrow 0)$ is the vector specifying the boundary conditions in the absence of chemical reactions, and $\underline{b}^{\text{sr}} = \underline{b}(\sigma \rightarrow 0)$ specifies the boundary conditions for an uncharged particle.

V. PROPULSION SPEED

Having determined the electrostatic potential, we calculate the fluid flow by making use of the Lorentz reciprocal theorem [7]. This allows one to transform the Stokes equation, Eq. (S5), from a 3D partial differential equation into an integral equation on the 2D domain boundary (the swimmer surface). Using this approach, a general formula for the propulsion velocity \mathbf{U} of a non-slip sphere generated by an axisymmetric distribution of force density \mathbf{f} has been derived [8]

$$\mathbf{U} = -\frac{\hat{\mathbf{z}}}{6\pi\eta a} \int_V \left[\left(\frac{3a}{2r} - \frac{a^3}{2r^3} - 1 \right) \cos\theta \hat{\mathbf{r}} - \left(\frac{3a}{4r} + \frac{a^3}{4r^3} - 1 \right) \sin\theta \hat{\theta} \right] \cdot \mathbf{f} dV, \quad (\text{S36})$$

where the volume integral is over the region outside the sphere, and the scalar speed U used in the main text is defined by $\mathbf{U} = U\hat{\mathbf{z}}$. In our case, $\mathbf{f} = \rho_e \nabla\phi$.

For a uniformly charged sphere, the equilibrium potential distribution is

$$\phi^{\text{eq}} = \frac{\sigma a^2 e^{-\kappa(r-a)}}{r\epsilon(1+\kappa a)}. \quad (\text{S37})$$

Making the usual assumption of a small driving field, i.e., $\phi^{\text{sr}} \ll \phi^{\text{eq}}$ gives in this case a speed

$$U = \frac{2\sigma}{3\eta a} \sum_j \frac{\kappa - g_j}{(\kappa + g_j)^2} \phi_{j,1}^{\text{sr}} F(\kappa a, g_j a), \quad (\text{S38})$$

where the $\phi_{j,1}^{\text{sr}}$ are to be read out from Eq. (S35) and

$$F(x, y) = \frac{(x+y)^3}{6(1+x)(1+y)} e^{x+y} \times \int_1^\infty \frac{(t-1)^2(2t+1)}{t^5} (1+xt)(1+yt) e^{-t(x+y)} dt, \quad (\text{S39})$$

which is the self-electrophoretic equivalent of the Henry function for electrophoresis in an external field [9]. We have verified that Eq. (S38) is also obtained by solving the 3D Stokes equations directly, applying Henry's methods for electrophoresis in an external field [5, 9, 10].

VI. THE EQUIVALENCE OF ELECTROSTATIC BOUNDARY CONDITIONS

In this section, we show that a particle with fixed, uniform surface charge σ has the same propulsion velocity as an equivalent particle with fixed, uniform surface potential ζ , as long as

$$\zeta = \frac{\sigma a}{\epsilon(1+\kappa a)}. \quad (\text{S40})$$

To do this, we first need to show that modifying the electrostatic boundary conditions of the particle has only a limited effect on the fields of concentration and potential; namely, that such modifications can only introduce electrostatic fields corresponding to the equilibrium Debye-Hückel solutions around passive colloids.

We take a swimmer, in a given chemical environment, and apply to it three sets of boundary conditions. Boundary conditions (1) and (2), with corresponding solutions $\underline{y}^{(1)}$ and $\underline{y}^{(2)}$, have equal chemical flux boundary conditions (equal surface reaction rates), but have arbitrary, different electrostatic boundary conditions. Boundary condition (3) consists of a no flux condition on all species (no surface reactions), and the electrostatic boundary condition

$$y_0^{(3)}(\mathbf{s}) = y_0^{(2)}(\mathbf{s}) - y_0^{(1)}(\mathbf{s}). \quad (\text{S41})$$

Since there are no fluxes through this particle's surface, each chemical species is in equilibrium, and the solution to this boundary condition is just the equilibrium, Debye-Hückel solution

$$y_i^{(3)} = \begin{cases} \frac{e\psi}{k_B T}, & i = 0, \\ -\frac{ez_i\psi}{k_B T}, & i = 1, 2, \dots, N', \end{cases} \quad (\text{S42})$$

where the equilibrium potential field ψ must satisfy both the electrostatic boundary condition, Eq. (S41), and the Debye-Hückel equation $\nabla^2\psi = \kappa^2\psi$. One can then show by direct substitution of Eq. (S42) into Eq. (S14), that the solutions to the three boundary problems are related by $\underline{y}^{(2)} - \underline{y}^{(1)} = \underline{y}^{(3)}$. In particular, $\phi^{(2)} - \phi^{(1)} = \psi$, which implies

$$\nabla^2 [\phi^{(2)} - \phi^{(1)}] = \kappa^2 [\phi^{(2)} - \phi^{(1)}]. \quad (\text{S43})$$

Hence the difference $\phi^{(2)} - \phi^{(1)}$ between the electric potential fields of particles (1) and (2) corresponds to the equilibrium Debye-Hückel solutions around a passive colloid.

As before, we make the assumption of a small driving field, $\phi^{\text{sr}} \ll \phi^{\text{eq}}$, where $\phi = \phi^{\text{eq}} + \phi^{\text{sr}}$. Now, consider two particles (1') and (2'), with equal surface reactions, but where (1') has uniform surface charge density σ , and (2') has uniform surface potential ζ , with σ and ζ satisfying

Eq. (S40). In this case, the two equilibrium fields are equal, i.e., $\phi^{(1')\text{eq}} = \phi^{(2')\text{eq}}$, and are given by Eq. (S37). Inserting this equality into Eq. (S43) yields

$$\nabla^2 [\phi^{(2')\text{sr}} - \phi^{(1')\text{sr}}] = \kappa^2 [\phi^{(2')\text{sr}} - \phi^{(1')\text{sr}}]. \quad (\text{S44})$$

In other words, the difference in the reaction-generated electrostatic potential field between (1') and (2') is an equilibrium, Debye-Hückel type field, which has an inverse screening length $g_j = \kappa$. From the $(\kappa - g_j)$ term in Eq. (S38), we see that such a field can have no effect on the propulsion speed. This proves our initial assertion that, to linear order, a particle with fixed, uniform surface charge σ will have the same propulsion velocity as an equivalent particle with fixed, uniform surface potential ζ , as long as Eq. (S40) is satisfied.

In fact, one can make a more general statement, which we will not prove. For any two particles (1') and (2'), with equal arbitrary shape, surface reactions, and equilibrium (possibly non-uniform) fields ϕ^{eq} , not only the propulsion speed but the entire flow field will be the same. A physical justification for this conclusion is that if the interaction between one equilibrium field (ϕ^{eq}) and another (the difference field between (1') and (2')) could generate fluid flow, then this would constitute a perpetual-motion machine. Analogous conclusions also apply to electrophoresis in an external field [11].

VII. ESTIMATION OF IONIC RATE CONSTANTS

An important parameter in our calculations is the ionic reaction association constant k_{as} in the reaction $\text{H}^+ + \text{HO}_2^- \rightleftharpoons \text{H}_2\text{O}_2$ in water. We were unable to find a value for this constant in the literature, so we must estimate it. Fortunately, reactions involving the transfer of a proton or a hydroxyl ion, such as this one (and most of the reactions involved in similar systems), are normally sufficiently fast to be diffusion limited [12]. It has been shown [13], that the diffusion-limited rate constant between two species, A and B , with diffusivities D_A , D_B , and valencies z_A , z_B , which react at a short distance r_{AB} is [14]

$$k_{\text{as}} = [4\pi(D_A + D_B)r_{AB}] f(z_A z_B, r_{AB}). \quad (\text{S45})$$

Here, $f(z_A z_B, r_{AB})$ is a modifier for charged species, given by

$$f = \frac{z_A z_B e^2}{4\pi\epsilon r_{AB} k_B T} \left[\exp\left(\frac{z_A z_B e^2}{4\pi\epsilon r_{AB} k_B T}\right) - 1 \right]^{-1}. \quad (\text{S46})$$

For reactions involving neutral species, $f(0, r_{AB}) = 1$, giving the rate expression originally derived by Smoluchowski [15]. For reactions between oppositely charged species, over a typical reaction distance in water of $r_{AB} = 0.2 \text{ nm}$ [14], $f(-1, r_{AB}) = 3.59$. For the reaction between H^+ (species A) and HO_2^- (species B), this

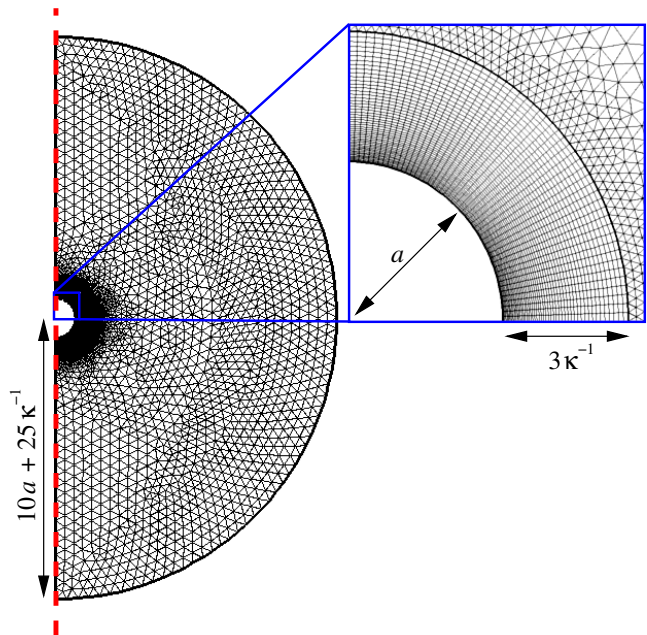


FIG. S1. The mesh on which the FEM calculations are performed. This particular mesh was generated for radius $a = 0.5 \mu\text{m}$ and a salt concentration of 10^{-5} mol/L , but illustrates the generic features of all the meshes. The rotational symmetry of the simulation domain is exploited to calculate on a quasi-2D domain: the symmetry axis is indicated by the dashed red line. The domain typically has a radius $L = 10a + 25\kappa^{-1}$ in size. This domain is subdivided into two pieces on which triangular and quadrilateral elements are used. In a range of $3\kappa^{-1}$ around the colloid the domain consists of quadrilaterals, which grow in size geometrically, see the zoom-in (blue box). Beyond this range the elements are triangular and are allowed to grow out linearly to best fit the domain boundary and reduce the overall number of elements.

yields, using the diffusivities quoted in the main text, $k_{\text{as}} = 4.9 \times 10^{10} \text{ M}^{-1} \text{ s}^{-1}$.

As a check on this value, we note that it is consistent with measured rates for similar reactions [12], i.e., $\text{H}^+ + \text{HCO}_3^- \rightleftharpoons \text{H}_2\text{CO}_3$ in water has $k_{\text{as}} = 5 \times 10^{10} \text{ M}^{-1} \text{ s}^{-1}$ [16].

VIII. FINITE ELEMENT METHOD CALCULATIONS

To verify the linear, analytic calculations presented in Sections II-VI, we numerically solve the full non-linear system of equations presented in Section I using the finite element method (FEM). FEM calculations are performed using the COMSOL Multiphysics Modelling package.

We employed the following strategies to accelerate the calculations and obtain high quality results. (i) The solutions were obtained in a 2D cylindrically symmetric geometry. (ii) We ignored the advective coupling term in Eq. (S1). This allowed us to split the problem into

TABLE I. The first Legendre components of the surface flux densities, and the charge densities, used in Fig. 3 in the main text and Fig. S3 here. The flux densities have units $\text{mol}/(\text{m}^2\text{s})$, and the charge densities have units e/nm^2 . The final column gives the product of σ and the relevant non-zero flux density, with units $\text{emol}/(\text{m}^2\text{nm}^2\text{s})$.

Fig.	Type	$j_{\theta,1}^s$	$j_{+,1}^s$	$j_{-,1}^s$	σ	σj^s
3	I	3×10^{-1}	0	0	10^{-4}	3×10^{-5}
	II	0	3×10^{-7}	0	10^{-4}	3×10^{-11}
	III	0	3×10^{-5}	3×10^{-5}	10^{-4}	3×10^{-9}
S3	I	1.5×10^{-2}	0	0	10^{-2}	1.5×10^{-4}
	II	0	1.5×10^{-5}	0	10^{-2}	1.5×10^{-7}
	III	0	1.5×10^{-5}	1.5×10^{-5}	10^{-2}	1.5×10^{-7}

electrostatics plus hydrodynamics parts, as for the linear theory, and thus solve the uncoupled equations more efficiently. This approach is justified, since the Péclet number (Pe) $\lesssim 10^{-2}$ for typical experimental systems ($Pe = aU/D$, where a is the colloidal radius, U is the typical magnitude of the flow field, and D is a molecular diffusivity). We also verified this directly, by including the advective coupling term in a subset of the data points, finding good agreement. (iii) We created a physics-specific mesh, see Fig. S1, on which we solved the system. Quadrilateral elements were used out to a distance of $3\kappa^{-1}$ from the colloid surface. These elements grow exponentially in size with increasing distance, whilst maintaining a constant number along the tangential direction. The remainder of the domain was meshed with triangular elements which grow larger with distance from the colloid. (iv) The following polynomial orders were employed for the test functions: electrostatics (3), diffusion (5) and hydrodynamics (2+3). These higher orders proved necessary to reduce spurious flow (see also Ref. [3]). (v) Finite-size scaling was employed to check for artifacts arising from the finite extent of the simulation domain. (vi) Mesh refinement was used for several simulations to determine the dependence of our result on the element size. (vii) We also varied the tolerance on the residual for a few cases to verify that our solutions had sufficiently converged.

To verify the analytic results, we first performed calculations with sufficiently low values of the surface charge density and flux to remain in the linear regime (Fig. 3, main text). These values are given in Table I. Different fluxes were used for the different propulsion models because the low efficiency of type I and III propulsion mean that numerical errors become significant more quickly as the flux density is reduced for these models. In addition, the FEM calculations and the linearized theory produce essentially identical electrostatic potential fields. Fig. S2a illustrates this for type II electrophoresis. Theory and FEM calculations differ at the boundary of the simulation domain (Fig. S2b) because the FEM calculations have an artificial equipotential boundary there.

However, the potential and flow-fields decay sufficiently rapidly that this does not affect the potential near the particle, or the propulsion speed beyond a few percent.

We can also use the FEM to go beyond the linear approximation. We defer to future work a systematic investigation of the non-linear behaviour, and here focus on the propulsion speed for selected experimentally relevant values of the surface charge density and chemical fluxes. These values are taken from measurements on the Pt-polystyrene Janus swimmers in Ref. [17], and are listed in Table I, in the ‘S3’ section. The neutral flux density $j_{\theta,1}^s$ is that which would be produced by a Janus particle which uniformly consumes H_2O_2 on one hemisphere at a rate $\Gamma = 8 \times 10^{10}$ molecules per second per particle. This rate was measured for $a = 1 \mu\text{m}$ radius particles in 3 M H_2O_2 [17]. The surface charge density is taken from the electrophoretic mobility measurements made on the same particles in Ref. [18]. The ionic fluxes are unknown, but we arbitrarily set $j_{\pm,1}^s = 10^{-3}j_{\theta,1}^s$, so that type II electrophoresis gives a speed of order $100 \mu\text{ms}^{-1}$, which is larger than typical experimental values for Au-Pt spherical microswimmers [19, 20]. Hence, our results should overestimate the non-linear behaviour of the propulsion speed. Note that though the ionic flux densities for the experimentally realistic case are sometimes lower than those for the linear case, the product of charge density and surface flux is always greater in the experimentally realistic case, Table I.

Figure S3a-b, both with 1 mM NaCl, correspond to Fig. 3a-b in the main text. We see that the analytical theory continues to match the FEM calculations well even for these realistic values of the flux and charge densities. However, many experiments are performed with no added salt, and as shown in Fig. S3c, this agreement worsens as the salt concentration falls. This is to be expected, since it is low salt that generates a high- ζ , large-screening-length regime where linear approximations break down [21]. In fact, with 0 mM NaCl, the

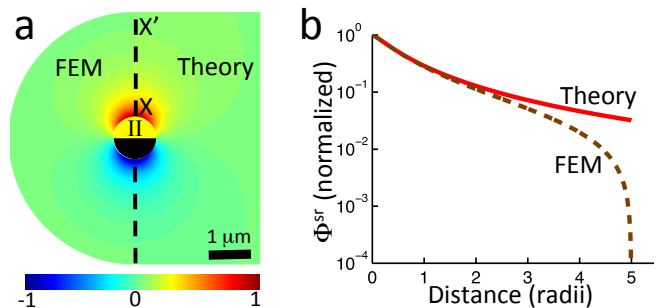


FIG. S2. a) Comparison of normalized surface-reaction-generated potential fields ϕ^{sr} for (left) FEM and (right) linearized theory, for type II self-electrophoresis, with $j_{+,1}^s = 3 \times 10^{-7} \text{ mol}/(\text{m}^2\text{s})$, and with other conditions as in the base parameter set (see main text). The radius of the simulation domain $L = 3 \mu\text{m} = 6a$ here. b) Normalized radial decay of ϕ^{sr} for linearized theory (—) and FEM calculations (---) along X-X' in a.

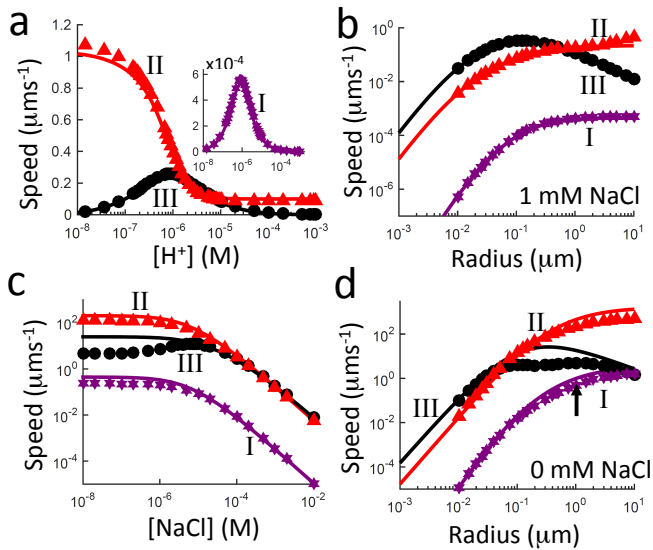


FIG. S3. Propulsion speed for realistic parameters (given in this text) for type I (★, inset), II (▲), and III (●) propulsion, from analytical theory (solid curves) and FEM simulations (symbols). For a) $[H^+]$ at fixed κ equivalent to 1 mM NaCl, b) particle radius with 1 mM NaCl c) NaCl concentration, d) particle radius with 0 mM NaCl. In d, the black arrow indicates the experimental point from Ref. [17] referred to in the text.

dimensionless zeta-potential $\zeta e/(k_B T) = 5.6$ for these particles, well beyond the Debye-Hückel limit. Nevertheless, for type I-II propulsion, the agreement remains semi-quantitative between simulations and theory over the whole radius range for 0 mM NaCl, Fig. S3d.

From Fig. S3d, we obtain a speed of $0.5 \mu\text{ms}^{-1}$ for type I electrophoresis with particles of radius $a = 1 \mu\text{m}$, no salt, and 3 M H_2O_2 (the black arrow indicates the relevant datapoint). As stated in the main text, this predicted speed can account for at most 5% of the experimentally measured propulsion speed of $15 - 20 \mu\text{ms}^{-1}$ obtained for Pt-Polystyrene Janus particles under the same conditions [17].

-
- [1] J. L. Anderson, *Ann. Rev. Fluid Mech.* **21**, 61 (1989).
 [2] J. F. Brady, *J. Fluid. Mech.* **667**, 216 (2011).
 [3] J. de Graaf, G. Rempfer, and C. Holm, *IEEE Trans. Nanobiosci.* **14**, 272 (2015).
 [4] J. L. Moran and J. D. Posner, *Phys. Fluids* **26**, 042001 (2014).
 [5] J. Y. Kim and B. J. Yoon, *J. Colloid Interf. Sci.* **262**, 101 (2003).
 [6] K. F. Riley, M. P. Hobson, and S. J. Bence, *Mathematical methods for physics and engineering: a comprehensive guide*, Cambridge University Press, 2006.
 [7] B. Sabass and U. Seifert, *J. Chem. Phys.* **136**, 064508 (2012).
 [8] M. Teubner, *J. Chem. Phys.* **76**, 5564 (1982).
 [9] D. Henry, *Proc. Roy. Soc. Lond. A Mat.* **133**, 106 (1931).
 [10] S. Kim and S. J. Karrila, *Microhydrodynamics: principles and selected applications*, Courier Dover Publications, 2013.
 [11] R. W. O'Brien and L. R. White, *J. Chem. Soc.- Faraday T.* **2** **74**, 1607 (1978).
 [12] E. Caldin, *Fast reactions in solution*, Blackwell Scientific Publications, Oxford, 1964.
 [13] P. Debye, *T. Electrochem. Soc.* **82**, 265 (1942).
 [14] K. J. Laidler, editor, *Chemical Kinetics, 3rd ed.*, Harper Collins, New York, U.S.A., 1987.
 [15] M. Von Smoluchowski, *Z. Phys.* **17**, 557 (1916).
 [16] Y. Pocker and D. W. Bjorkquist, *J. Am. Chem. Soc.* **99**, 6537 (1977).
 [17] A. T. Brown and W. C. K. Poon, *Soft Matter* **10**, 4016 (2014).
 [18] A. T. Brown et al., *Soft Matter Advance Article*, DOI: 10.1039/C5SM01831E (2015).
 [19] P. M. Wheat, N. A. Marine, J. L. Moran, and J. D. Posner, *Langmuir* **26**, 13052 (2010).
 [20] I. Theurkauff, C. Cottin-Bizonne, J. Palacci, C. Ybert, and L. Bocquet, *Phys. Rev. Lett.* **108**, 268303 (2012).
 [21] R. J. Hunter, *Foundations of colloid science*, Oxford University Press, 2001.